

# Calculation of the $N$ to $\Delta$ electromagnetic transition matrix element \*

C. Alexandrou<sup>a</sup>, Ph. de Forcrand<sup>b</sup>, Th. Lippert<sup>c</sup>, H. Neff<sup>†d</sup>, J. W. Negele<sup>e</sup>, K. Schilling<sup>c</sup> and A. Tsapalis<sup>c</sup>

<sup>a</sup>Department of Physics, University of Cyprus, CY-1678 Nicosia, Cyprus

<sup>b</sup>ETH-Zürich, CH-8093 Zürich and CERN Theory Division, CH-1211 Geneva 23, Switzerland

<sup>c</sup>Department of Physics, University of Wuppertal, D-42097 Wuppertal, Germany

<sup>d</sup>Institute of Accelerating Systems and Applications and Department of Physics, University of Athens, Athens, Greece

<sup>e</sup>Center for Theoretical Physics, Laboratory for Nuclear Science and Department of Physics, Massachusetts Institute of Technology, Cambridge, Massachusetts 02139 U.S.A

We present results on the ratio of electric quadrupole to magnetic dipole amplitudes,  $R_{EM} = \mathcal{G}_{E2}/\mathcal{G}_{M1}$ , for the transition  $\gamma N \rightarrow \Delta$  from lattice QCD. We consider both the quenched and the 2-flavor theory.

## 1. INTRODUCTION

Accurate experimental measurements of transition matrix elements  $N \rightarrow \Delta$  [1,2] give strong support for a deformed nucleon and/or  $\Delta$ . On the lattice, hadron wave functions [3] can provide information on the deformation of particles of spin higher than 1/2. For a spin 1/2 particle however, the quadrupole moment vanishes, and this is the reason why one turns to measurements of quadrupole strength in the  $\gamma N \rightarrow \Delta$  transition as in experimental studies. State-of-the-art lattice QCD calculations can yield accurate results on these matrix elements and provide direct comparison with experiment. Spin-parity selection rules allow a magnetic dipole, M1, an electric quadrupole, E2, or a Coulomb quadrupole, C2, amplitude. If both the nucleon and the  $\Delta$  are spherical then E2 and C2 are expected to be zero. Although M1 is indeed the dominant amplitude there is mounting experimental evidence for a range of momenta transfer that E2 and C2 are non-zero [1,2]. The physical origin of non-zero E2 and C2 amplitudes is attributed to different mechanisms in the various models. In quark models the deformation is due to the colour-magnetic

tensor force. In “cloudy” baryon models it is due to meson exchange currents. By comparing quenched and unquenched results we aim at an understanding of the origin of a non-zero deformation.

A previous lattice QCD study [4] of the  $N \rightarrow \Delta$  transition with a limited number of quenched configurations yielded an inconclusive result for the ratio,  $R_{EM}$ , of E2 to M1 amplitudes, since a zero value could not be statistically excluded. In this work we improve by using smearing techniques to have cleaner plateaus, a larger lattice and more configurations. Moreover, we present first full QCD results, based on the SESAM lattices [5].

## 2. LATTICE MATRIX ELEMENTS

The current matrix element for  $N \rightarrow \Delta$  transitions with on-shell nucleon and  $\Delta$  states and real or virtual photons has the form [6]

$$\langle \Delta(p', s') | J_\mu | N(p, s) \rangle = i \sqrt{\frac{2}{3}} \left( \frac{M_\Delta M_N}{E'_\Delta E_N} \right)^{1/2} \bar{u}_\tau(p', s') \mathcal{O}^{\tau\mu} u(p, s) . \quad (1)$$

The operator  $\mathcal{O}^{\tau\mu}$  can be decomposed as

$$\mathcal{G}_{M1}(q^2) K_{M1}^{\tau\mu} + \mathcal{G}_{E2}(q^2) K_{E2}^{\tau\mu} + \mathcal{G}_{C2}(q^2) K_{C2}^{\tau\mu} , \quad (2)$$

\*Talk presented by A. Tsapalis

†Acknowledges funding from the European network ESOP (HPRN-CT-2000-00130) and the University of Cyprus.

where the magnetic dipole,  $\mathcal{G}_{M1}$ , electric quadrupole,  $\mathcal{G}_{E2}$ , and scalar quadrupole,  $\mathcal{G}_{C2}$ , form factors depend on the momentum transfer  $q^2 = (p' - p)^2$ . The kinematical functions  $K^{\tau\mu}$  depend on  $p$ ,  $p'$ ,  $M_N$  and  $M_\Delta$  and their expressions are given in [6]. Following [4] we calculate the three-point correlation functions

$$\begin{aligned} \langle G_\sigma^{\Delta j^\mu N}(t_2, t_1; \vec{p}', \vec{p}; \Gamma) \rangle &= \\ \sum_{\vec{x}_2, \vec{x}_1} \exp(-i\vec{p}' \cdot \vec{x}_2) \exp(+i(\vec{p}' - \vec{p}) \cdot \vec{x}_1) \\ \Gamma^{\beta\alpha} \langle \Omega | T \left[ \chi_\sigma^\alpha(\vec{x}_2, t_2) j^\mu(\vec{x}_1, t_1) \bar{\chi}^\beta(\vec{0}, 0) \right] | \Omega \rangle \end{aligned} \quad (3)$$

and  $\langle G_\sigma^{N j^\mu \Delta}(t_2, t_1; \vec{p}', \vec{p}; \Gamma) \rangle$ . For the spin- $\frac{1}{2}$ ,  $\chi^p(\vec{x}, t)$ , and  $-\frac{3}{2}$ ,  $\chi_\sigma^{\Delta^+}(\vec{x}, t)$ , interpolating fields and projection matrices  $\Gamma$  we use the expressions given in ref. [4].

For large Euclidean time separations  $t_2 - t_1 \gg 1$  and  $t_1 \gg 1$ , the time dependence and field normalization constants are cancelled in the following ratio [4]

$$\begin{aligned} R_\sigma(t_2, t_1; \vec{p}', \vec{p}; \Gamma; \mu) &= \\ \left[ \frac{\langle G_\sigma^{\Delta j^\mu N}(t_2, t_1; \vec{p}', \vec{p}; \Gamma) \rangle \langle G_\sigma^{N j^\mu \Delta}(t_2, t_1; -\vec{p}, -\vec{p}'; \Gamma^\dagger) \rangle}{\langle -g_{ij} G_{ij}^{\Delta\Delta}(t_2, \vec{p}'; \Gamma_4) \rangle \langle G^{NN}(t_2, -\vec{p}; \Gamma_4) \rangle} \right]^{1/2} \\ \sim \left( \frac{E_N + M_N}{2E_N} \right)^{1/2} \left( \frac{E'_\Delta + M_N}{2E'_\Delta} \right)^{1/2} \bar{R}_\sigma(\vec{p}', \vec{p}; \Gamma; \mu) \end{aligned} \quad (4)$$

We use the lattice conserved electromagnetic current,  $j^\mu(x)$ , symmetrized on site  $x$  by taking  $j^\mu(x) \rightarrow [j^\mu(x) + j^\mu(x - \hat{\mu})]/2$ .

In the laboratory frame we take  $\vec{p} = 0$  and  $\vec{p}' = \vec{q} = (q, 0, 0)$ . The Sachs form factors can be extracted from the plateau values of  $\bar{R}_\sigma(\vec{p}', \vec{p}; \Gamma; \mu)$  for specific combinations of matrices  $\Gamma$  and  $\sigma$  as in ref. [4]. For example,  $R_{EM}$  is given by

$$R_{EM} = \frac{1}{3} \frac{\{\bar{R}_3(\vec{q}, 0; \Gamma_1; 3) + \bar{R}_1(\vec{q}, 0; \Gamma_3; 3)\}}{\{\bar{R}_3(\vec{q}, 0; \Gamma_1; 3) - \bar{R}_1(\vec{q}, 0; \Gamma_3; 3)\}}. \quad (5)$$

Smearing is essential for filtering the ground state before the signal from the time correlators is lost in the noisy large time limit. We use the gauge invariant Wuppertal smearing in order to increase the overlap with the baryon states. Quark propagators with a photon insertion are computed with the sequential source technique.

We also implement the equal re-weighting of  $\{U\}$  and  $\{U^*\}$  gauge configurations in the lattice action [7]. Fig 1 shows that fluctuations are substantially reduced at large time separations resulting in better plateaus for  $\bar{R}_\sigma(\vec{p}', \vec{p}; \Gamma; \mu)$ . This greatly overbalances the fact that an additional sequential propagator with momentum  $(-q, 0, 0)$  is required.

### 3. RESULTS

For the quenched analysis we used 100 gauge configurations on a lattice of size  $32^3 \times 64$  at  $\beta = 6.0$ . We take  $u$  and  $d$  quarks of the same mass. The lowest momentum transfer on this lattice is  $q^2 \approx 0.14 \text{ GeV}^2$ , close to the value of  $q^2 = 0.126 \text{ GeV}^2$  where an accurate measurement of  $R_{EM} = (-2.1 \pm 0.2_{\text{stat}} \pm 2.0_{\text{mod}})\%$  was recently obtained [1]. Note that the statistical error is an order of magnitude smaller than the ‘model’ estimated error involved in the extraction of this ratio. A reliable result from lattice QCD is thus a valuable input. A photon is injected at  $t_1/a = 8$ , allowing enough time for filtering out excited baryonic states. Jackknife averages and  $\chi^2$  fits are performed on the plateaus.  $R_{EM}$  at  $\kappa = 0.1558$  is shown in Fig. 2. The best fit to the plateau yields  $R_{EM} = (-0.9 \pm 0.8)\%$  with  $\chi^2/\text{d.o.f} \sim 0.4$ .

If deformation is due to the pion cloud, unquenching should make the ratio  $R_{EM}$  more negative. We analysed 100 SESAM configurations for a lattice of size  $16^3 \times 32$  at  $\beta = 5.6$  at four different values of sea quark mass. The results are given in the Table. The analysis was done at the lowest possible momentum transfer for this lattice,  $q^2 \sim 0.53 \text{ GeV}^2$  (taking  $a^{-1} = 1.85 \text{ GeV}$  from the chiral extrapolation of the nucleon mass).

$\kappa_{\text{sea}}$	$m_\pi/m_\rho$	$R_{EM}(\%)$	$R_{SM}(\%)$
0.1560	0.83	$-2.24 \pm 0.46$	
0.1565	0.81	$-2.25 \pm 0.55$	
0.1570	0.76	$-3.40 \pm 0.61$	$-3.2 \pm 2.1$
0.1575	0.69	$-2.98 \pm 0.90$	

The measured  $R_{EM}$  as a function of the sink time-slice  $t_2$  is shown in Fig. 3 for  $\kappa_{\text{sea}} = 0.1570$ . We obtain a very clear plateau at a negative value. Moreover, this value, in the  $(-2 \text{ to } -3)\%$

range, is in agreement with the recently measured experimental value of  $-1.6 \pm 0.4 \pm 0.4$  at a similar momentum transfer [2]. Considering that the experimental value of  $R_{EM}$  changes little from  $q^2 = 0.126$  GeV $^2$  to  $q^2 = 0.52$  GeV $^2$ , we expect that the main difference between our quenched and unquenched results comes from dynamical quark contributions pointing to pionic cloud contributions to the deformation. For the unquenched case we have also measured the ratio of C2 to M1 amplitudes,  $R_{SM}$ , which involves the time component of the electromagnetic current. In Fig. 4 we show this ratio as a function of time. The C2 amplitude is extracted from the three combinations  $\bar{R}_1(\vec{q}, 0; -i\Gamma_1; 4)$ ,  $\bar{R}_2(\vec{q}, 0; i\Gamma_2; 4)$  and  $\bar{R}_3(\vec{q}, 0; i\Gamma_3; 4)$ . As it can be seen all three yield consistent results. Fitting to the common plateau we obtain a negative non-zero result indicating baryon deformation.

In summary, using state-of-the-art lattice techniques the phenomenologically important  $R_{EM}$  and  $R_{SM}$  values can be extracted for various  $q^2$  values. Unquenching drives both ratios more negative and yields results that are consistent with experimental measurements.

## REFERENCES

- [1] C. Mertz *et al.*, Phys. Rev. Lett. **86** (2001) 2963.
- [2] K. Joo *et al.*, Phys. Rev. Lett. **88** (2002) 122001.
- [3] C. Alexandrou, Ph. de Forcrand and A. Tsapalis, hep-lat/0206026; these proceedings.
- [4] D. B. Leinweber, T. Draper and R. M. Woloshyn, Phys. Rev. D **48**, (1993) 2230.
- [5] N. Eicker *et al.*, Phys. Rev. D **59** (1999) 014509.
- [6] H. F. Jones and M.C. Scadron, Ann. Phys. (N.Y.) **81**, 1 (1973)
- [7] T. Draper, W. Wilcox, R. M. Woloshyn and K. F. Liu, Nucl. Phys. B **318**, (1989) 319; Nucl. Phys. B (Proc. Suppl.) **9**, (1989) 175.

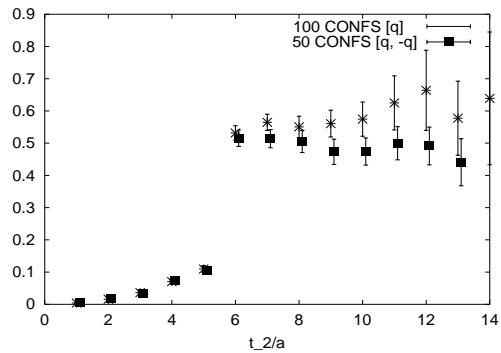


Figure 1. Noise reduction in  $\bar{R}_3(\vec{q}, 0; \Gamma_1; 3)$  by equal  $U$ ,  $U^*$  weighting in the action for 100 SESAM configurations at  $\kappa = 0.1570$ ,  $t_1/a = 6$  and  $a$  is the lattice spacing.

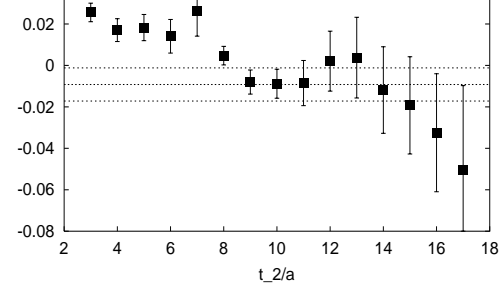


Figure 2.  $R_{EM}$  at  $\kappa = 0.1558$  for 100 quenched confs. The photon is injected at  $t_1/a = 8$ .

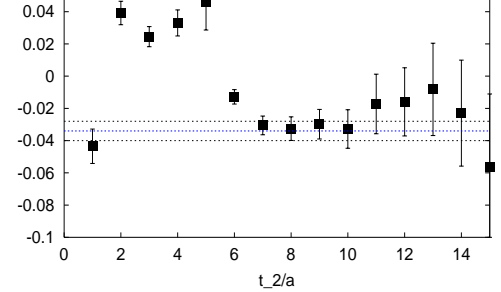


Figure 3.  $R_{EM}$  ratio for 100 SESAM confs. at  $\kappa = 0.1558$ . The photon is injected at  $t_1/a = 6$ .

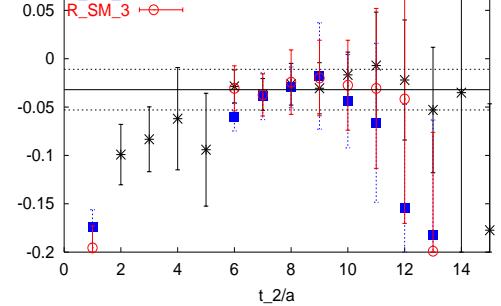


Figure 4.  $R_{SM}$  plateaus for 100  $\kappa = 0.1570$  SESAM lattices. The three equivalent definitions are consistent within the errors.  $t_1/a = 6$ .